DIFFRACTIVE PROTON–PROTON SCATTERING IN HOLOGRAPHIC QCD*

Alexander Stoffers, Ismail Zahed

Department of Physics and Astronomy, Stony Brook University
Stony Brook, NY 11794, USA

(Received January 14, 2013)

We further analyze the holographic dipole–dipole scattering amplitude developed in G. Basar *et al.*, *Phys. Rev.* **D85**, 105005 (2012) and A. Stoffers, I. Zahed, `arXiv:1205.3223 [hep-ph]`. Gribov diffusion at strong coupling yields the scattering amplitude in a confining background. We compare the holographic result for the differential cross section to diffractive proton–proton scattering data.

DOI:10.5506/APhysPolBSupp.6.7
PACS numbers: 13.90.+i, 12.38.Lg

1. Introduction

In [1, 2] a holographic version of the dipole–dipole scattering approach [3] in the Regge limit is used to describe high energy hadron–hadron scattering within the context of holographic QCD. In this limit, the scattering amplitude is dominated by pomeron exchange, *i.e.* exchange of ordered gluon ladders with vacuum quantum number. The holographic pomeron is argued [1, 2, 4] to be the exchange of a non-critical, closed string in transverse AdS_3. Within the gauge/gravity duality, hadron–hadron scattering and the holographic pomeron have been discussed in numerous places, see *e.g.* [5].

Using the dipole–dipole scattering approach, two Wilson loops are correlated via a minimal surface with string tension $\sigma_{\rm T}$. In the presence of a large rapidity gap χ and large impact parameter b, the closed string exchange is T-dual to an open string exchange subjected to a longitudinal 'electric' field $E = \sigma_{\rm T}\,\tanh(\chi/2)$ that causes the oppositely charged string end-points to accelerate [1]. This acceleration induces an Unruh temperature $T_{\rm U} \approx \chi/2\pi b$ in the middle of the string work-sheet. For large impact parameter, the Unruh temperature is low and only the tachyon mode of the non-critical

* Presented at the Light Cone 2012 Conference, Kraków, Poland, July 8–13, 2012.

string is excited. This tachyonic string mode is diffusive in curved AdS_3, which is reminiscent of Gribov's diffusion in QCD. In particular, the properly normalized diffusion kernel with suitable boundary conditions in the infrared yields a *wee-dipole* density that is similar to the QCD one in the conformal limit. The convolution of the two *wee-dipole* densities yields the eikonalized scattering amplitude and allows for a 'partonic' picture similar to [6], albeit at strong coupling. We will use the holographic dipole–dipole scattering model, [1, 2], to describe proton–proton (pp) diffraction and compare our results to data from ISR and LHC.

2. Diffractive scattering as dipole–dipole scattering

In the dipole–dipole scattering approach at high energies ($\chi = \ln(\frac{s}{s_0}) \gg 1$), the scattering amplitude for the process $a\,p \to c\,p$ factorizes and can be written as

$$\mathcal{T}(\chi, \boldsymbol{b}_\perp) = \int_0^\infty du \int_0^\infty du' \psi_a^*(u)\psi_p^*\left(u'\right) \mathcal{T}_{\rm DD}\left(\chi, \boldsymbol{b}_\perp, u, u'\right) \psi_b(u)\psi_p\left(u'\right)\ , \tag{2.1}$$

with transverse impact parameter $\boldsymbol{b}_\perp$, rapidity χ and dipole–dipole amplitude $\mathcal{T}_{\rm DD}$. The wave functions ψ are parametrized by $u = -\ln(z/z_0)$, with the effective dipole size z and the IR cutoff z_0. The dipole–dipole amplitude is evaluated using the gauge/gravity duality and the virtuality of the scatterers is identified with the holographic direction of the curved space [2, 7].

In the eikonal approximation the differential cross section reads

$$\begin{aligned}
&\frac{d\sigma_{ap\to cp}}{dt}(\chi, |t|) = \frac{1}{16\pi s^2}|\mathcal{T}(\chi, |t|)|^2 \\
&= \frac{1}{4\pi}\left| i\int d\boldsymbol{b}_\perp \int du \int du'\ e^{iq_\perp\cdot\boldsymbol{b}_\perp}\ |\psi_{ab}(u)|^2 \left|\psi_p\left(u'\right)\right|^2 \left(1 - e^{\boldsymbol{WW}}\right)\right|^2 \\
&= \frac{\pi}{4}\left| i\int d|\boldsymbol{b}_\perp|^2 \int du \int du'\ J_0\left(\sqrt{|\boldsymbol{b}_\perp|^2|t|}\right)\ |\psi_{ab}(u)|^2 \left|\psi_p\left(u'\right)\right|^2 \left(1 - e^{\boldsymbol{WW}}\right)\right|^2
\end{aligned} \tag{2.2}$$

with $t = -q_\perp^2$. Here, J_0 is the Bessel function and the overlap amplitude is defined by $|\psi_{ab}(u)|^2 \equiv \psi_a^*(u)\psi_b(u)$. In [1, 2] the eikonal $\boldsymbol{WW}$, which is the correlator of two Wilson loops, was obtained through closed string exchange in a weakly curved, confining space. The string exchange can be viewed as a funnel connecting the two dipoles at a holographic depth z and z'. Identifying these positions z, z' of the endpoints of the funnel with the effective size of the dipoles gives rise to a density $\boldsymbol{N}$ of *wee-dipoles* surrounding each parent dipole. For $D_\perp = 3$, we identify [2]

$$\boldsymbol{WW} \approx -\frac{g_s^2}{4}\left(2\pi\alpha'\right)^{3/2} zz' \, \boldsymbol{N}\left(\chi, z, z', \boldsymbol{b}_\perp\right) . \tag{2.3}$$

We consider transverse AdS$_3$, $ds_\perp^2 = \frac{1}{z^2}(d\boldsymbol{b}_\perp^2 + dz^2)$, with a cutoff imposed at some z_0. The *effective* string tension will be defined as $g_s \equiv \kappa \frac{1}{4\pi\alpha'^2 N_c} \equiv \kappa \frac{\lambda}{4\pi N_c}$, with t' Hooft coupling λ and $\alpha' = 1/(2\pi\sigma_{\mathrm{T}}) \equiv 1/\sqrt{\lambda}$ the string tension (in units of the AdS radius). N_c is the number of colors and the parameter κ is fixed by the saturation scale, see [2]. The density reads

$$\boldsymbol{N}\left(\chi, \boldsymbol{b}_\perp, z, z'\right) = \frac{1}{zz'}\,\Delta(\chi, \xi) + \frac{z}{z' z_0^2}\,\Delta(\chi, \xi_*)\,, \tag{2.4}$$

and the heat kernel Δ in the AdS$_3$ background is given by

$$\Delta_\perp(\chi, \xi) = \frac{e^{(\alpha_P - 1)\chi}}{(4\pi\boldsymbol{D}\chi)^{3/2}} \frac{\xi e^{-\frac{\xi^2}{4\boldsymbol{D}\chi}}}{\sinh(\xi)}\,, \tag{2.5}$$

with the chordal distances $\cosh\xi = \cosh(u' - u) + \frac{1}{2}\boldsymbol{b}_\perp^2\, e^{u'+u}$, $\cosh\xi_* = \cosh(u' + u) + \frac{1}{2}\boldsymbol{b}_\perp^2 e^{u'-u}$. To leading order in $1/\sqrt{\lambda}$ the pomeron intercept and the diffusion constant read $\alpha_P = 1 + \frac{D_\perp}{12} - \frac{(D_\perp - 1)^2}{8\sqrt{\lambda}}$, $\boldsymbol{D} = \frac{\alpha'}{2} = \frac{1}{2\sqrt{\lambda}}$.

In order to confront the holographic result for the differential proton–proton cross section with the data, we have to fix the parameters entering the eikonal $\boldsymbol{WW}$ in (2.3). In [2] a comparison of the proton structure function F_2 to DIS data determined the following numerical values. N_c was set to 3 and the onium mass taken to give $s_0 = 0.1\,\mathrm{GeV}^2$. The value of the coupling, $\lambda = 23$, is fitted through the slope of the proton structure function F_2 in comparison to the DIS data. Phenomenological considerations on the saturation scale gives $\kappa = 2.5$. These numerical values will be used in the following analysis.

3. Proton–proton scattering

Diffractive proton–proton scattering at small momentum transfer unravels information about the transverse shape of the proton and the large $|t|$ behavior probes lengths scales of the typical string length, which in the confining background is of the order of z_0. We will fit the effective dipole size of the proton, z_p, and the position of the hard wall, z_0, to the data.

We will fit the data assuming the proton distribution is identified with the *wee-dipole* distribution, *i.e.* the proton is sharply peaked at some scale $1/z_p$. More explicitly, the square of the wave function will be approximated by a delta-function, $|\psi_p(u)|^2 = \mathcal{N}_p\, \delta(u-u_p)$. We treat the normalization constant $\mathcal{N}_p$ that carries the dipole distribution to the physical proton distribution as a parameter to be fitted to the data. A comparison of the differential elastic pp cross section, (2.2), to the CERN ISR data [8] is made by fitting the position of the dip and the slope of the shoulder region ($|t| > 1.5\,\mathrm{GeV}^2$). For a comparison to a wider energy range and further details, see [9]. A fit yields $z_0 = 2\,\mathrm{GeV}^{-1}$, $z_p = 3.3\,\mathrm{GeV}^{-1}$ and $\mathcal{N}_p = 0.16$, see figure 1. To leading order, the position of the (first) dip is sensitive to the effective size of the scatterer and the energy of the scattering object and scales with $1/(\boldsymbol{D}\chi z_p^2)$. The fit with $z_p > z_0$ is larger than the cutoff set by the hard-wall at z_0. This shortfall is readily fixed by considering a smooth wall which is also more appropriate for describing hadron resonances [10].

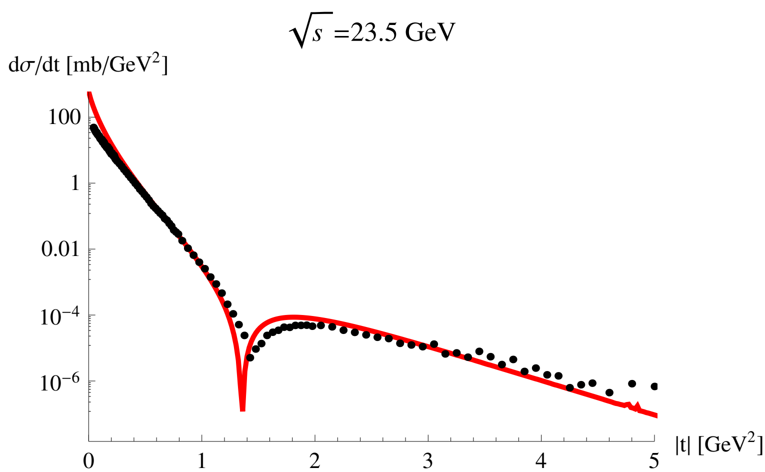

Fig. 1. Differential pp cross section. Dots: data from CERN ISR. Solid line: holographic result. See the text.

At high momentum transfer ($|t| > 2\,\mathrm{GeV}^2$), the typical length scales probed are of the size of the fundamental string length, which is of the order of the IR cutoff. Thus, the slope of the shoulder region is fitted by primarily adjusting the value of the confinement scale z_0. The result for the cross section in the conformal limit $z_0 \to \infty$ does not yield a reasonable fit to the data. We note that unlike perturbative QCD reasoning, [11], where the partons are resolved at large $|t|$ leading to a power-like decrease, the slope of the cross section at $|t| \geq 2\,\mathrm{GeV}^2$ is essentially not power-like in our holographic model.

In the approach taken here, the transverse structure of the proton is modeled by a cloud of *wee-dipoles* surrounding a parent dipole. We can easily understand the scaling of the proton size with the coupling. As the coupling increases, the outer part of the cloud becomes more dilute and the proton shrinks.

Elastic pp scattering at LHC energies of $\sqrt{s} = 7\,\mathrm{TeV}$, allows us to test the energy dependence of our model. With the numerical values fitted at energies $\sqrt{s} \sim 20$–$60\,\mathrm{GeV}$, the fit in figure 2 indicates a miss match in the energy dependence of the holographic model. In order to get a better fit to the LHC data, the parameters governing the overall strength (κ), the position of the dip (z_p) and the slope of the shoulder (z_0) are adjusted. The fit (dashed/blue line) in figure 2 is obtained with $\kappa = 3.75$, $z_p = 3.1\,\mathrm{GeV}^{-1}$, $z_0 = 1.5\,\mathrm{GeV}^{-1}$, while the fit (gray dotted/red) uses the values from figure 1, $\kappa = 2.5$, $z_p = 3.3\,\mathrm{GeV}^{-1}$, $z_0 = 2\,\mathrm{GeV}^{-1}$. This new parameter set for the LHC data is overall consistent with the set for the ISR data.

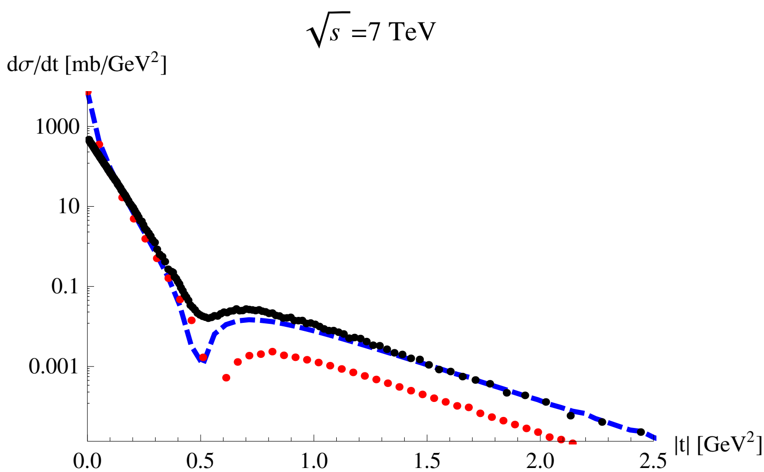

Fig. 2. Differential pp cross section. Black dots: data from the TOTEM experiment at LHC, [12]. Dashed/blue line and gray/red dots: holographic result. See the text.

4. Conclusions

The parameters of the model developed in [1] were fitted against DIS data in [2]. In order to refine the numerical values characterizing the proton shape and the IR cutoff, we have confronted the differential cross section with data on pp scattering. High energy hadronic scattering is dominated by pomeron exchange. Due to its non-perturbative nature at strong coupling, the holographic pomeron admits Gribov diffusion in curved space. Within the dipole–dipole scattering approach, the holographic description allows to access the saturation regime at small Bjorken x and small momentum transfer.

We have been able to get a reasonable fit to the pp scattering data and obtained a refinement of the effective dipole size z_p of the proton. The slope of the cross section in the region $|t| > 2\,\mathrm{GeV}^2$ is sensitive to the IR cutoff scale, indicating the necessity of a confining background. However, the hard wall seems to be a too crude approximation for an IR cutoff. In order to fit the pp data, we need $z_p \geq z_0$ suggesting that the smooth-wall background [10] is a more suitable setup. While the hard-wall construct allows for explicit and analytical results, the smooth-wall construct is likely numerical and will be addressed elsewhere.

REFERENCES

[1] G. Basar, D.E. Kharzeev, H.-U. Yee, I. Zahed, *Phys. Rev.* **D85**, 105005 (2012) [arXiv:1202.0831 [hep-th]].

[2] A. Stoffers, I. Zahed, arXiv:1205.3223 [hep-ph].

[3] A.H. Mueller, *Nucl. Phys.* **B335**, 115 (1990); N.N. Nikolaev, B.G. Zakharov, *Z. Phys.* **C49**, 607 (1991); G.P. Salam, *Nucl. Phys.* **B449**, 589 (1995) [arXiv:hep-ph/9504284].

[4] A. Stoffers, I. Zahed, arXiv:1211.3077 [nucl-th].

[5] M. Rho, S.-J. Sin, I. Zahed, *Phys. Lett.* **B466**, 199 (1999) [arXiv:hep-th/9907126]; R.A. Janik, R.B. Peschanski, *Nucl. Phys.* **B565**, 193 (2000) [arXiv:hep-th/9907177]; R.C. Brower, J. Polchinski, M.J. Strassler, C.I. Tan, *J. High Energy Phys.* **0712**, 005 (2007) [arXiv:hep-th/0603115]; L. Cornalba, M.S. Costa, J. Penedones, *Phys. Rev. Lett.* **105**, 072003 (2010) [arXiv:1001.1157 [hep-ph]]; S.K. Domokos, J.A. Harvey, N. Mann, *Phys. Rev.* **D80**, 126015 (2009) [arXiv:0907.1084 [hep-ph]].

[6] S.J. Brodsky, G.F. de Teramond, *Phys. Rev. Lett.* **96**, 201601 (2006) [arXiv:hep-ph/0602252]; S.J. Brodsky, *Eur. Phys. J.* **A31**, 638 (2007) [arXiv:hep-ph/0610115].

[7] J. Polchinski, M.J. Strassler, *Phys. Rev. Lett.* **88**, 031601 (2002) [arXiv:hep-th/0109174]; J. Polchinski, M.J. Strassler, *J. High Energy Phys.* **0305**, 012 (2003) [arXiv:hep-th/0209211].

[8] U. Amaldi, K.R. Schubert, *Nucl. Phys.* **B166**, 301 (1980).

[9] A. Stoffers, I. Zahed, arXiv:1210.3724 [nucl-th].

[10] A. Karch, E. Katz, D.T. Son, M.A. Stephanov, *Phys. Rev.* **D74**, 015005 (2006) [arXiv:hep-ph/0602229].

[11] I.M. Dremin, arXiv:1206.5474 [hep-ph].

[12] G. Antchev *et al.*, CERN-PH-EP-2012-239, Aug 2012.